



Synthesis of phytoextract-mediated Ag-doped graphitic carbon nitride (Ag@GCN) for photocatalytic degradation of dyes

Sweety Dahiya¹ · Anshu Sharma² · Sudesh Chaudhary¹

Received: 3 August 2022 / Accepted: 11 January 2023 / Published online: 25 January 2023
© The Author(s), under exclusive licence to Springer-Verlag GmbH Germany, part of Springer Nature 2023

Abstract

The present work focuses on the green synthesis of Ag-doped graphitic carbon nitride (Ag@GCN) for photocatalytic activities, which can contribute to a more sustainable environment. The leaf extract of the *Ocimum tenuiflorum* (Tulsi) plant was used to prepare the silver nanoparticles, as the plant extract serves as a stabilizing and capping agent in producing silver nanoparticles. Both Ag nanoparticles and urea-derived GCN were synthesized by thermal polymerization. The Ag-doped GCN nanocomposites were synthesized using various millimolar concentrations of Ag nanoparticles (NPs) with a fixed amount of GCN. The green nanocomposites (NCs) were synthesized by calcinating leaf extract at about 550 °C. They were then characterized for surface morphology by SEM coupled with energy-dispersive X-ray spectroscopy (EDX), and elemental composition by XRD, Fourier-dispersive infrared spectroscopy (FTIR), and transmission electron microscope (TEM). Thermal stability and estimation of the Ag content in GCN were done through thermogravimetric analysis. The prepared series of nanocomposites (Ag-doped GCN 0.5 mM, 1.0 mM, 1.5 mM, 2.0 mM) were used to study the photocatalytic degradation efficiency of rose bengal (RB) and xylene orange (XO) dyes. The degradation efficiency of dyes gets enhanced due to the doping of Ag nanoparticles into GCN. The efficiency increased from 54 to 76% and 15 to 36% in the case of RB and XO dyes, respectively. The apparent rate constant value increased up to 2.5 times in the case of the Ag-doped GCN (1.5 mM) nanocomposite in comparison to GCN. The result obtained from the study confirmed that Ag-doped GCN (1.5 mM) could act as a potential photocatalyst for wastewater remediation applications.

Keywords Green synthesis · Leaf extract · Photocatalytic activity · Synthetic dyes · Nanocomposites

Introduction

Environmental pollution is one of the world's most prevalent issues today (Gaballah et al. 2020). These days rapid population growth and the unavailability of pure water supplies have become a global problem. Water contamination also

adds to it and is caused by various factors, including industrial discharge, pesticide overuse, fertilizer use in agriculture, pharmaceutical residue, and residential trash landfilling (Bhatia et al. 2017). The industrial sector releases a wide range of organic pollutants, many of which are difficult to break down, like chlorophenols, pesticides, polychlorinated biphenyls (PCBs), dioxins, dibenzofurans, and dyes (Wang et al. 2008). Since many industries are based on dye, their wastewater discharge contains an enormous amount of dye, which is a substantial pollutant (Ahmed et al. 2016; Cuerdo-correa et al. 2020). These organic dyes from industrial waste, like many other organic contaminants, cause a substantial problem because of their potential toxicity to aquatic organisms and have severe consequences on human health, plants, and aquatics (Wang et al. 2014). The organic dyes are persistent towards light, heat, and other chemical reactions.

Dye contamination in wastewater can be easily identified since even a minute amount of synthetic dye in water (one part per million) is highly apparent, altering the aesthetic

Responsible Editor: Sami Rtimi

✉ Sudesh Chaudhary
sudesh.energy@dcrustm.org

Anshu Sharma
anshusharda@gmail.com

¹ Centre of Excellence for Energy and Environmental Studies, Deenbandhu Chhotu Ram University of Science and Technology, Murthal, Sonapat 131039, Haryana, India

² Department of Physics Under School of Engineering and Technology, Central University of Haryana, Mahendergarh 123031, Haryana, India

value and clarity of water bodies (Karagolge and Gur 2016; Sharma et al. 2021). They absorb and scatter the sunlight that enters the water, impeding the growth of aquatic species and preventing photosynthesis (Qu et al. 2013). Furthermore, depending on the concentration and period of exposure, they could have acute and chronic impacts on organisms. Thus, it is essential to degrade dye in wastewater before being released into the environment (Buzea et al. 2007).

Various physical, chemical, biological, and acoustical treatments are utilized to combat textile dye pollution in the environment (Ahmed et al. 2016). These techniques primarily separate and remove the dyes from water but face some difficulties like insufficient decolorization, costly technology and monitoring equipment, high reagent or energy requirements, and the formation of hazardous sludge and other waste (Singh et al. 2018). Advanced oxidation processes (AOP) have recently focused on dye removal from wastewater. Photocatalysis is an advanced oxidation methodology that combines light with photocatalytic elements. The band gap, surface area, and generation of electron–hole pairs are the main determinants of the photocatalytic activity of materials for destroying dyes present in water. The study of the surface area is essential for photocatalytic dye degradation as higher surface area results in more dye molecules adhering to the photocatalyst's surface and thus increases the photocatalytic activity. A semiconductor material that absorbs a photon with the same energy as its band gap is known as a photocatalyst. This semiconductor material generates electron–hole pairs, which are then separated and transported to the target pollutant for the redox process (Martín-Ramos et al. 2015). It also has excellent chemical and thermal stability (Meng et al. 2011). However, impeded marginal light absorption and surface area are two main variables that might reduce graphitic carbon nitride's (GCN) efficacy in visible light (Liu et al. 2020). Among other modification techniques, one of the most influential and convenient approaches is the formation of composites between GCN and other metal oxide semiconductors, which can resolve the drawbacks of rapid recombination of photogenerated charge carriers while trying to improve the photocatalyst's response to light (Rattan Paul and Nehra 2021; Shoran et al. 2022).

Noble metals such as Ag, Au, and Pt have been widely studied due to their outstanding antibacterial and dye degradation activity (Daupor and Chenea 2017). Silver nanomaterials have received specific attention because of their unique physical, chemical, and biological characteristics compared to bulky elements (Paul et al. 2019). Furthermore, due to its outstanding chemical stability, and electrical and optical properties, silver (Ag) is one of the most popular dopant choices (Ge et al. 2011). In contrast, harmful by-products are

produced when toxic compounds are used during synthesis (Martín-Ramos et al. 2015). Physical methods require high energy to maintain high pressure and temperature, so chemical techniques are most commonly used. Although chemical and physical processes can be used to synthesize and manufacture pure, well-defined nanomaterials, they are cost-effective and harmful to the environment (Jadoun et al. 2021). To circumvent the drawbacks of chemical and physical approaches, researchers have turned to biological systems, which employ an environmentally safe strategy for nanoparticle production (Bhakya et al. 2016). These days plants appear to provide a much better platform for the production of nanoparticles because they are free of toxic chemicals. Also, a wide variety of natural biomolecules in plant extracts (flavonoids, terpenoids, tannin alkaloids, phenols, quinines) facilitate nanoparticle synthesis and eliminate the need to include any additional chemical for reducing or removing impurities (Singh et al. 2018). However, the proper utilization of the material is constrained due to numerous issues, such as its low specific surface area and high recombination rate of light-induced electron–hole pairs. To address these challenges, approaches such as creating hetero-structures, manufacturing copolymers, thermal etching, and doping with foreign elements have been explored to increase the photocatalytic performance of graphitic carbon nitride. The charge recombination kinetics in metal and semiconductors can be significantly expedited when silver nanoparticles (Ag-NPs) are deposited on the surface of semiconductor-based metal oxide (Katas et al. 2018).

This work aims to use *Ocimum sanctum* (Tulsi) leaf extract as a rapid and green synthesis method to synthesize pure Ag nanoparticles (NPs) and Ag-doped GCN nanocomposites. The phytochemical components in the plant extract help in the reduction and stabilization of nanoparticles. In addition, rose bengal and xylenol orange dyes were used to examine the photocatalytic activity of the pure GCN, Ag nanoparticles, and Ag-doped GCN nanocomposites. A series of Ag-doped GCN nanocomposites (NCs) were prepared at different conc. as 0.5 mM, 1.0 mM, 1.5 mM, and 2.0 mM to get NCs to study the photocatalytic activity. Compared to their pure and other composite forms, the Ag-doped GCN nanocomposite (1.5 mM) exhibits good photocatalytic properties.

Experimental and characterization

Synthesis route

For the preparation of leaf extract, 10 g of Tulsi leaves (TS) was chopped and placed in a 500-mL beaker with 40-mL

double-distilled water, and the mixture was heated at room temperature until the aqueous solution turned dark green. The supernatant was then filtered and stored at 4 °C for later use.

Graphitic carbon nitride was synthesized by thoroughly dissolving 10 g of urea in 10 mL of distilled water at 30 °C by constantly stirring till a clear solution was obtained (Paul et al. 2020). The solution so obtained was heated in a hot air oven at 100 °C for 1 h. The resulting powder was then placed in a covered porcelain crucible, sealed firmly to prevent gas leakage, and heated to 550 °C for 3 h at a rate of 20 °C/min in a muffle furnace. A fine powdered pure GCN was obtained by crushing the samples.

To synthesize Ag nanoparticles (NPs), 1 mM silver nitrate was dissolved in 50 mL of double-distilled water, and the mixture was agitated at room temperature for 1 h. Ten milliliters of Tulsi seed extract was added drop by drop to the preceding solution and a dark brown color appeared, indicating the beginning of the synthesis of Ag-NPs. The mixture was stirred for 2 h to complete Ag-NP synthesis (Panchal et al. 2019). The pellets were removed after 15 min of centrifuging the solution at 5000 rpm. The collected pellet was dried in a hot air oven for 4 h at 80 °C. The acquired samples were finally calcined at 500 °C for 3 h. The Ag-NPs so obtained were stored in an airtight container for further experimentation.

The nanocomposites were prepared by mixing 10 g of urea with Ag-NPs of concentration 0.5 mM, 1.0 mM, 1.5 mM, and 2.0 mM in 50 mL of distilled water. To this added 10 mL of tulsi seed extract dropwise. The earliest signal of Ag-doped GCN-NCs was a color change from translucent to light yellowish-brown for 0.5 mM, yellowish-brown for 1.0 mM, dark greenish-yellow for 1.5 mM, and greenish-brown for 2.0 mM. After stirring for 2 h, the precipitate was periodically cleaned with distilled water and acetone while centrifuging at 5000 rpm for 15 min. The precipitates were dried at 80 °C in a hot air oven for 4 h. After obtaining the samples, they were calcined at 550 °C for 3 h, producing four distinct color schemes: brown for 0.5 mM, pale yellow-brownish for 1.0 mM, greenish-brown for 1.5 mM, and dark greenish-brown for 2.0 mM further stored in an airtight container.

Structural and morphological characterizations

Different analytical techniques were employed to characterize the synthesized green NPs and NCs. The UV–vis spectrophotometer was used to examine the nanoparticle spectrum curve within the given range. To identify the phytochemicals involved in the capping, reduction, and stabilization of the nanoparticles, Fourier transforms infrared spectroscopy

(FTIR, Perkin Elmer FRONTIER) was used to analyze the bonding and functional groups present in synthesized nano-materials. X-ray diffraction [Bruker D8 Advance with CuK α radiation 1.5406 Å] in the range of $2\theta = 20\text{--}80$ °C was used to determine whether nanoparticles are crystalline or amorphous. Thermogravimetric analysis (Perkin Elmer TGA 4000) was carried out in an atmosphere of air by using the temperature range between 30 and 800 °C. FESEM (JEOL JSM-7610F Plus) was used to analyze samples of GCN, Ag-NPs, and nanocomposite materials to assess the surface morphology. The size distribution of silver (Ag) on the surface of g-C₃N₄ was studied with TEM (TECHNAI 200 kV). The composition of the Ag-doped GCN nanocomposites was examined using energy-dispersive X-ray spectroscopy (EDX) and elemental mapping.

Photocatalytic degradation study

To track the photocatalytic activities of the synthesized materials, the degradation of the dyes—rose bengal (RB) and xylene orange (XO)—was performed in the presence of direct sunlight. For the photodegradation experiment, 0.010 g of the photocatalyst was stirred in 100 mL of 10 ppm aqueous dye solution in 250 mL of a conical glass beaker. To reach adsorption–desorption equilibrium in the dye solution, the above solution was stirred in the dark for 30 min at room temperature. During the experiment, 5 mL of suspensions was collected at 15-min time intervals, then centrifuged to separate the photocatalyst, and analyzed for absorbance with a UV–vis spectrophotometer (range 400 to 800 nm). The impact of photocatalysis on dye degradation was examined using changes in the primary absorption peak's intensity. The photocatalytic degradation efficiency was calculated using Eq. 1:

$$E = \frac{1 - \frac{C}{C_0}}{100} \% \quad (1)$$

where C_0 is the adsorption/desorption equilibrium concentration of solution at time t_0 and C is the concentration of solution at time t .

Using the Langmuir–Hinshelwood simplified pseudo-first-order kinetic model, the apparent rate constant for the dye degradation process was calculated as shown in Eq. 2:

$$\ln\left(\frac{C_0}{C_t}\right) = k_{app}t = kKt \quad (2)$$

where t is time (in minutes), C is the dye concentration (mg/L), k_{app} is the apparent rate constant (min^{-1}), K is the dye's adsorption coefficient on the catalyst particles, and k is the reaction rate constant (min^{-1}).

Results and discussion

Here in this study, for the first time, we used a one-step green synthesis route to prepare Ag-doped GCN nanocomposites by reducing Ag-NPs with leaf extracts of *Ocimum tenuiflorum* (Tulsi). *Ocimum tenuiflorum* contains glycosides carvacrol, ursolic acid, tannins, rosmarinic acid, terpenoids, phenolic compounds, and flavonoids, which are responsible for the reduction of silver ions to Ag-NPs (Panchal et al. 2019). Tulsi leaf extract has been used in the present work for fabricating Ag-doped GCN nanocomposites at varied concentrations. We have also modified some preparation conditions of nanomaterials to achieve good results.

Structural analysis

XRD patterns of all the obtained samples, i.e., Ag-NPs, GCN, and Ag-doped GCN nanocomposites, are shown in Fig. 1. The peaks for the Ag-NPs were at 32.8, 38, 45.5, and 56.4 along with a minor peak at 66.7 whereas GCN showed a significant peak produced at 27.5, plain (002), representing the graphitic stacking of C_3N_4 in the GCN (Paul et al. 2019). The peak's intensity has dropped and shifted to a larger angle due to the doping of Ag-NPs, corresponding to (002) (Liu et al. 2016). As can be seen in Fig. 1, when Ag-doped GCN (2.0 mM) was added, the peak associated with (002) disappeared entirely. Only the peak caused by Ag-NPs was seen slightly. As the concentration of Ag-NPs has been rising gradually, no peak has been observed. Due to the negligible amount of dopant species in the initial urea, no peak was seen for Ag 0.5 mM, Ag 1.0 mM, and Ag 2.0 mM; the only peak seen for Ag 1.5 mM corresponds

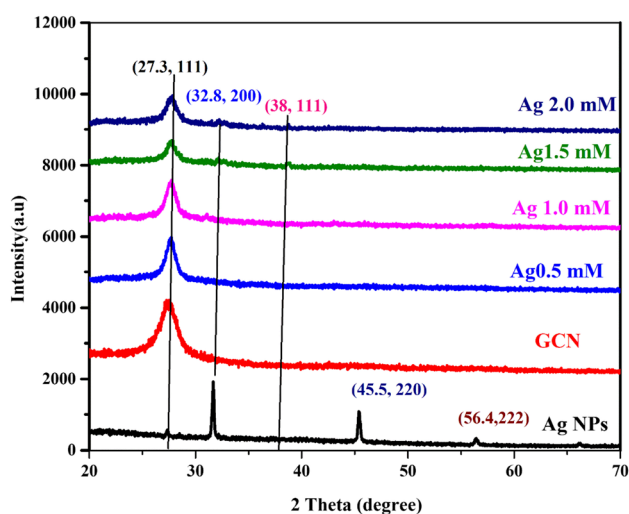


Fig. 1 XRD spectrum of Ag-Nps, GCN, and Ag-doped GCN NCs (at different conc.)

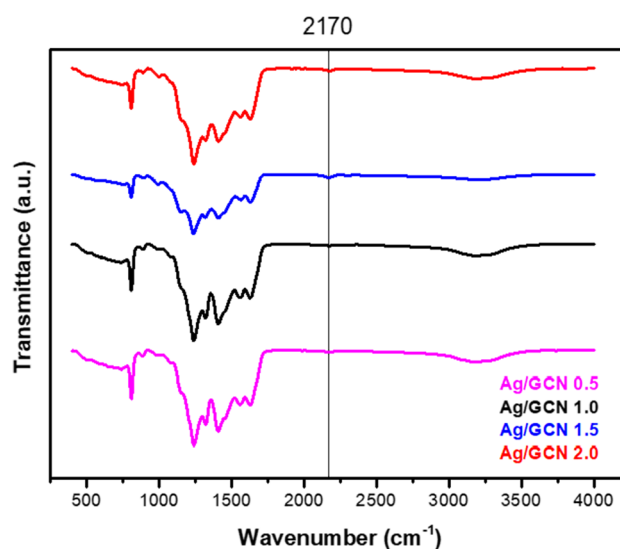


Fig. 2 FTIR spectra of Ag-doped GCN nanocomposites at various conc

to plain (111), related to Ag-NPs (200), (220), and (222) (Dai et al. 2017).

Figure 2 shows the FT-IR spectra of synthesized nanocomposites (NCs). In all samples, the peak was detected at 811 cm^{-1} , corresponding to triazine ring vibration breathing modes. The peaks observed between 1121 and 1699 cm^{-1} can be assigned to the stretching vibration of aromatic C-N and C-N heterocycles. The bandwidth between 3000 and 3500 cm^{-1} for all samples indicates the bending vibrations of NH and hydroxyl groups on the surface of a water molecule. It has been observed that when the conc. of Ag-NPs in the urea increases, the broadband's strength diminishes. In the case of Ag-doped GCN NCs (1.5 mM, 2.0 mM), the wide band at 3000 – 3500 cm^{-1} slightly disappeared. The intensity of the cyano group's peak at 2170 cm^{-1} increased gradually as the amount of Ag-NPs increased. As the amount of doped Ag increased, $sp^2\text{ C-N=C}$ and C=N were replaced by freshly generated $\text{C}\equiv\text{N}$. The addition of dopant caused most triazine units to break, indicating a significant binding between GCN and Ag-NPs, which may be explained by covalent bonding between the two, as per spectra of FTIR obtained.

Morphological analysis

FESEM at a voltage of 20 kV was used to examine the surface morphology of GCN, Ag nanoparticles, and Ag-doped GCN (1.5 mM NCs). Figure 3 shows FESEM images of GCN at 2 k; Ag nanoparticles at 5 k, 20 k, and 40 k; and Ag-doped GCN 1.5 mM NCs at 20 k and 40 k magnifications, respectively. All of the samples had a tremella-like structure, but the fluffiness of GCN decreased as Ag-NPs were doped

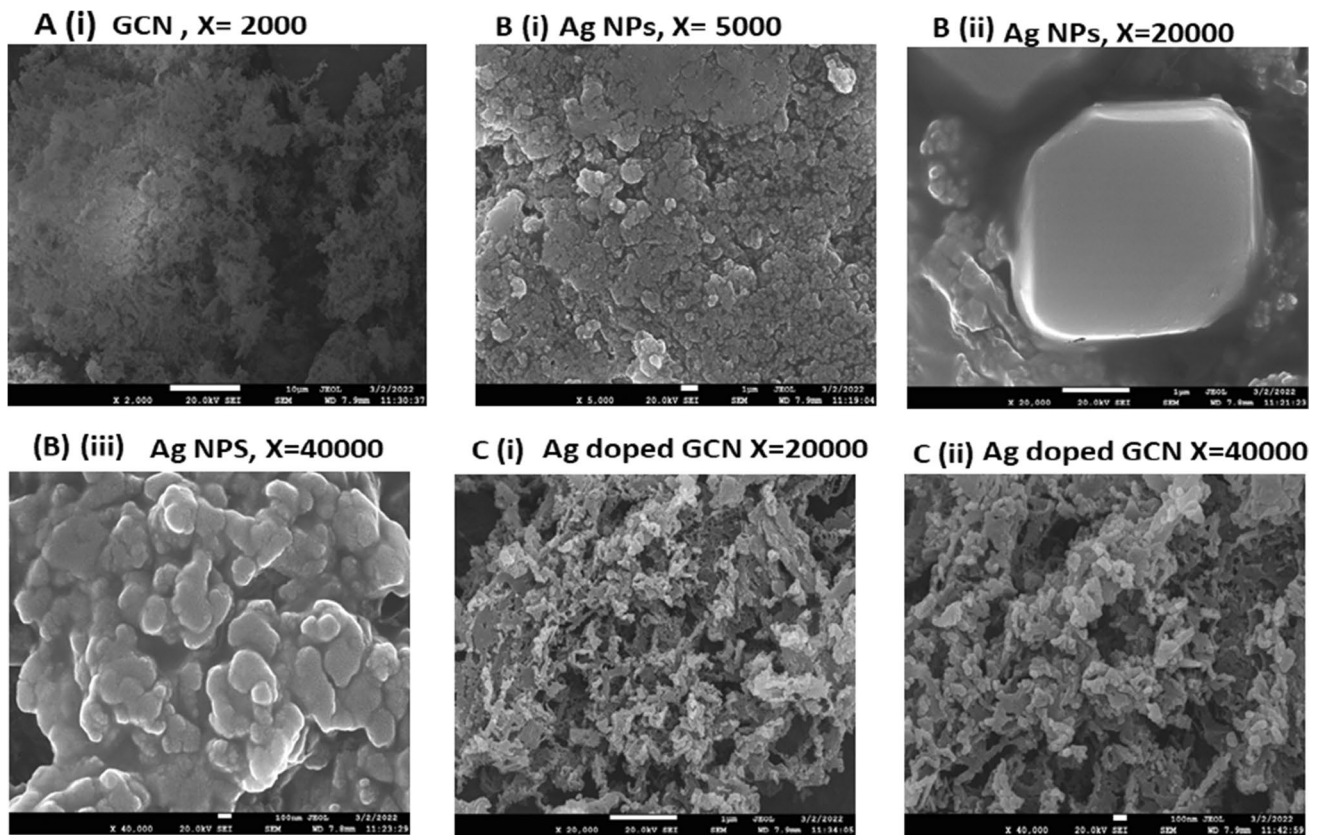


Fig. 3 FESEM of **a** GCN at 2k; **b** Ag-Nps at 5k, 20k, and 40k; and **c** Ag-doped GCN (1.5 mM NCs) at 20k and 40k

into it due to Ag nanoparticles forming on the surface of GCN. EDX examination revealed that the atomic % ratios of Ag, N, and C were 0.34, 27.08, and 72.58%, respectively, while the weight percent ratios of Ag, N, and C were 2.83, 29.46, and 67.72%, as shown in Fig. 4. Elemental mapping of the Ag-doped GCN (1.5 mM) samples revealed three elements (Ag, N, and C), which proved that the Ag-doped GCN 1.5 mM NCs composite were effectively generated. TEM images of GCN show the homogeneous distribution and fluffy nature. Big-size Ag-NPs were observed on the porous structure of GCN, as shown in Fig. 5.

UV–Vis optical study

The optical characteristics of GCN and Ag-doped GCN nanocomposites were examined using the UV–Vis diffused reflectance spectroscopy (DRS) method. The absorbance spectra revealed that the absorbance edges of pure GCN is at 384.1 nm and Ag-doped GCN nanocomposites are located at 440.7 nm, 485.6 nm, 514.2 nm, and 526.5 nm, respectively (Fig. 6). Ag-NPs doping altered the edge and enhanced the intensity of the absorption. The indirect band gaps of the samples were further calculated using

Kubelka–Munk method. After doping GCN with Ag-NPs, the band gap value decreased to 2.92 eV of GCN and to 2.81 eV, 2.67 eV, 2.48 eV, and 2.38 eV respectively of Ag-doped GCN nanocomposites. GCN's conduction and valance bands were caused by carbon (C; 2p) orbitals (Vinodkumar et al. 2019). The Ag-doped GCN (1.5 mM) showed the highest surface plasmon resonance phenomenon and strongest absorbance in direct sunlight (Ge et al. 2019; Zada et al. 2019). This may be due to the generation of more $e^- h^+$ pairs, which also strengthens its photocatalytic activity (Fan et al. 2018). Additionally, the band gap energy is reduced when Ag-NPs gradually replace the nitrogen in the triazine ring of GCN to generate composites.

Thermogravimetric analysis (TGA)

The thermal stability of GCN and Ag-doped GCN nanocomposite was estimated using TGA with a ramp rate of $10\text{ }^\circ\text{C min}^{-1}$ in temp. range of 30 to 800 $^\circ\text{C}$ and environment of air to explore the amount of Ag in GCN (Fig. 7). The initial weight loss occurred below 200 $^\circ\text{C}$, which may be due to volatilization of water or volatile contaminants

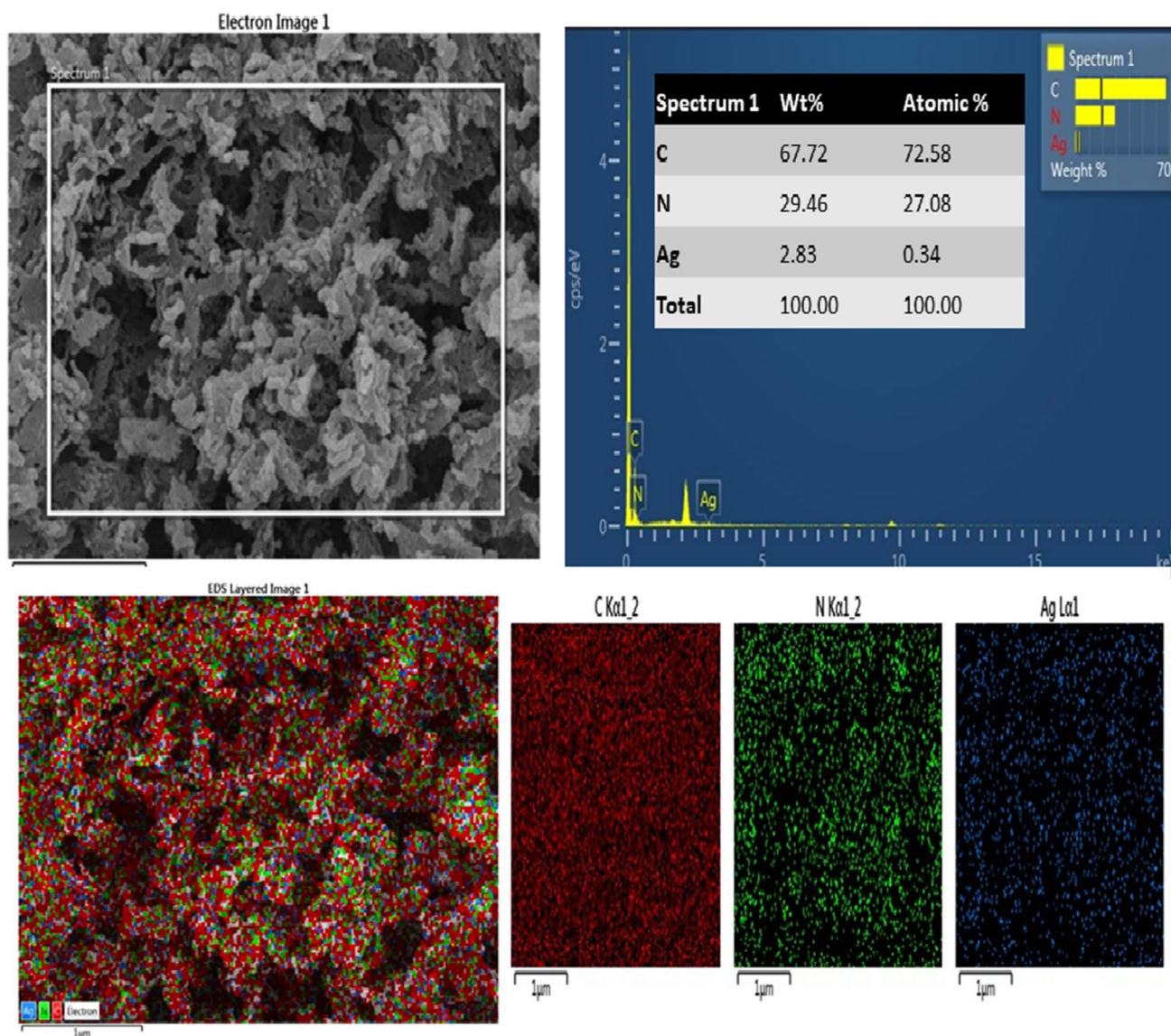


Fig. 4 EDX and elemental mapping of Ag-doped GCN 1.5mM NC

on the sample's surface. Further, GCN began to decompose at 530.2 °C and decomposed completely at 762.8 °C. Similar results were also observed for Ag-NPs and nanocomposites. The residual fraction weight was calculated for GCN and Ag-doped GCN nanocomposites (0.5 mM, 1.0 mM, 1.5 mM, 2.0 mM), which explains the Ag concentration in GCN as shown in Table 1.

Photocatalytic activity

The effects of silver doping on GCN as a photocatalyst were examined using the photocatalytic degradation process of RB and XO dye solution. The order of photocatalytic activity

potential was observed as Ag 1.5 mM > Ag 2 mM > Ag 1.0 mM > Ag 0.5 mM. The reduced activity of Ag-doped GCN (2.0 mM) may be due to an excess of $e^- h^+$ recombination sites, which might delay the transfer rate of photoinduced charges rather than having the maximum light absorption capacity. The significant degradation efficiency of GCN and nanocomposites was calculated with repetition of the experiment 3 times, as shown by the error bar graph in Fig. 8a and b. The photocatalytic activity of the Ag-doped GCN composites was higher than that of GCN, as shown in Figs. 9 and 10. The apparent rate constants (k) and % degradation efficiencies for GCN and nanocomposites have been shown in Table 2.

Fig. 5 TEM images of Ag-doped GCN nanocomposites (at 1.5mM conc.)

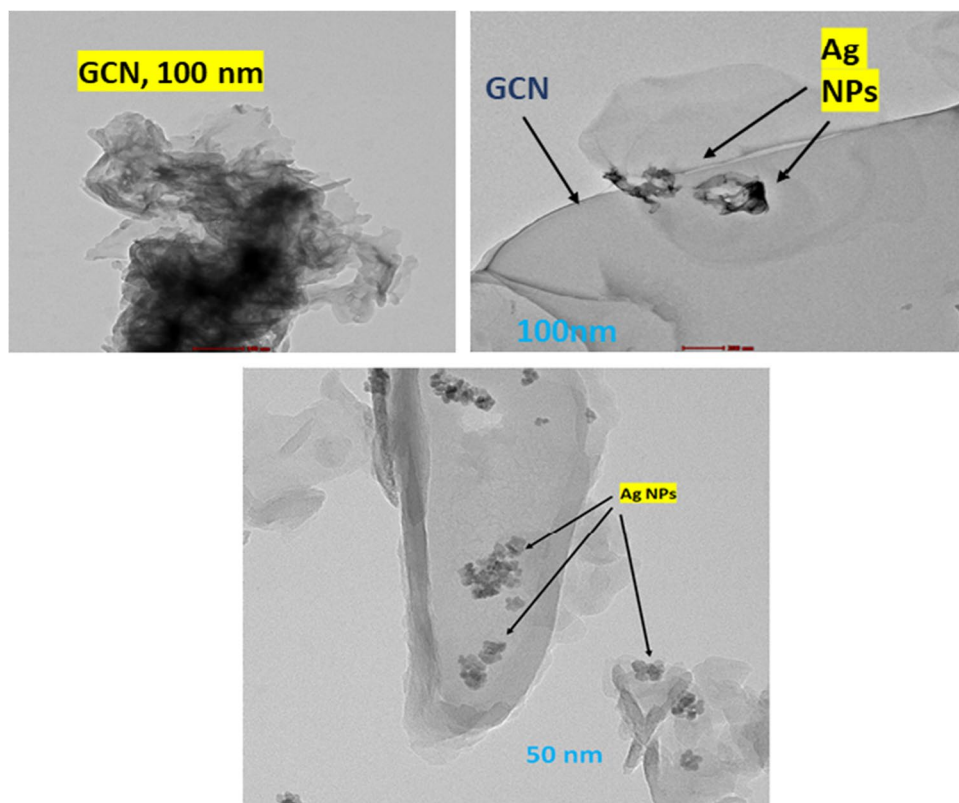
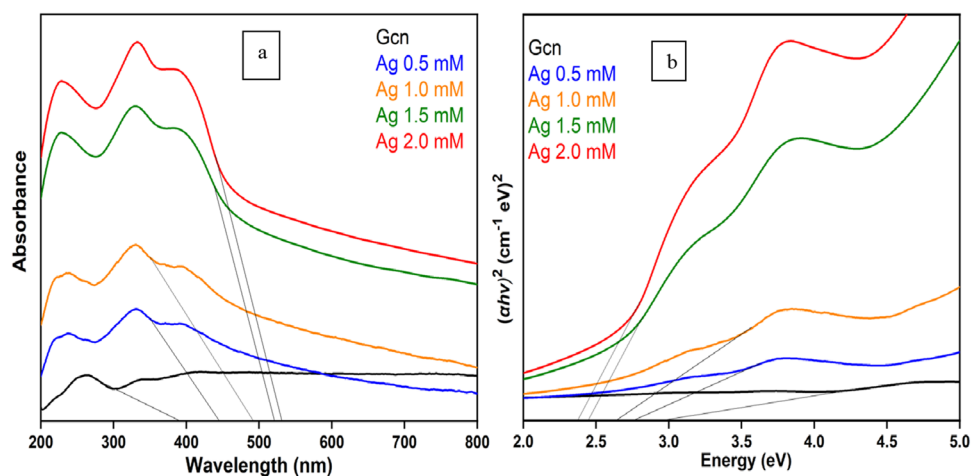


Fig. 6 **a** UV diffused reflectance spectra. **b** Tauc's plot for the calculation of band gap



Proposed mechanism for degradation

The Ag-doped GCN nanocomposites showed higher photocatalytic activity as compared to GCN. The doping of Ag-NPs in GCN accelerated the capacity of GCN to absorb visible light due to a reduction in band gap and an increase in surface area. In turn, it resulted in enhanced photocatalytic activity. As the light strikes the surface of GCN, the excited electrons in the valence band absorb the light and migrate to the conduction band, creating a hole in the valence band. Superoxide radicals are formed when oxygen

and free electrons combine, which can further photodegrade organic contaminants. The Ag-doped GCN nanocomposites provided a trapping site for photoinduced electrons and holes, as shown in Fig. 11. Based on observations, the addition of Ag-NPs to GCN has improved the photocatalytic activities due to reduced optical band gap, which might lead to more effective light trapping. In addition, the dopant atom (Ag) has a reduction potential of 0.80 V (Sengupta and Sarkar 2022), which is situated between the conduction band of graphitic carbon nitride (1.3 eV) and the valence band (+ 1.4 eV). As a result, a transient site for

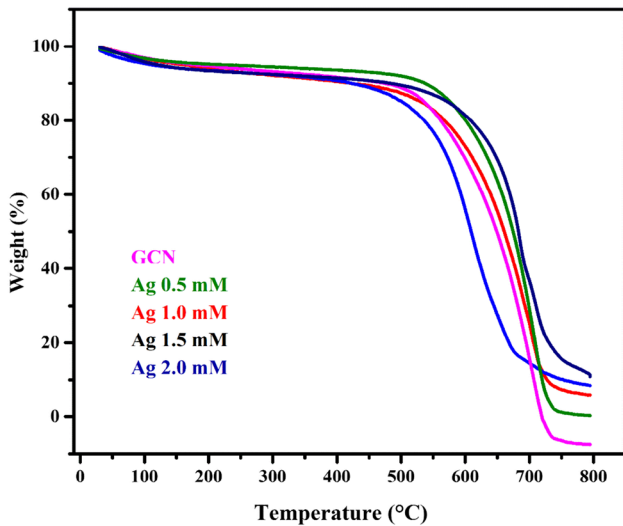


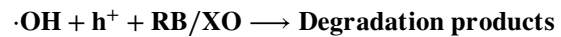
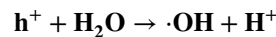
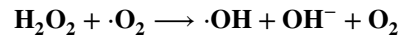
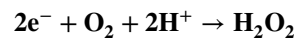
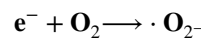
Fig. 7 TGA spectra of Ag-doped GCN nanocomposites at varied conc

Table 1 Percentage of residual weight in TGA

S. No.	Name of samples	Residual weight %
1.	GCN	00
2.	Ag 0.5 mM	2.70
3.	Ag 1.0 mM	4.96
4.	Ag 1.5 mM	11.20
5.	Ag 2.0 mM	8.40

trapping photogenerated electrons excited to the + 1.4 eV level is established. The electron acceptors, existing in the system or absorbed on the surface of GCN, such as O₂, react with trapped electrons, undergoing photoreduction to

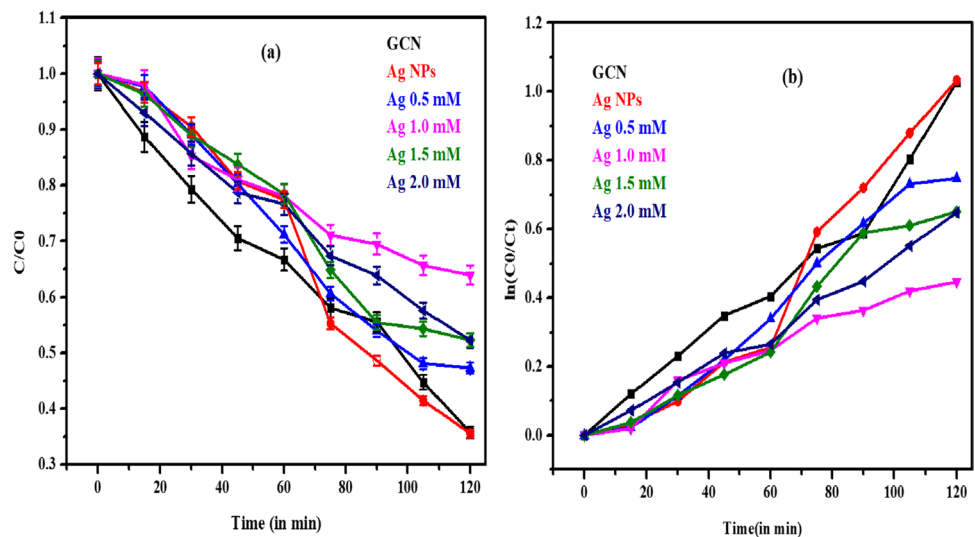
form reactive oxygen radicals ·O₂⁻. This is because the O₂/O₂⁻ redox potential lies at -0.33 eV. The redox potential of ·OH/OH⁻ lies at + 1.99, and therefore, the photogenerated holes on the GCN surface cannot react with ·OH – or H₂O molecules to form ·OH radicals (Cao et al. 2013). In turn, the holes in the valence band of Ag-NPs possibly oxidize the rose bengal dye, but in the case of xylenol orange, they caused hindrance to photoactivity due to insufficient electron-hole pair recombination. This improves the transfer of charge carriers, and the recombination of photo-generated e⁻ - h⁺ pairs is effectively delayed by Ag-NPs doping. This can be explained by the following reactions (Soltani et al. 2012):



Degradation efficiency comparison of anionic and cationic dye

In the presence of Ag-Nps as a catalyst, the absorption spectra for rose bengal and xylenol orange showed reduced peaks

Fig. 8 a RB and XO dye degradation comparison. **b** ln(C₀/C_t) as a function of visible light irradiation time with Ag-doped GCN nanocomposites and GCN



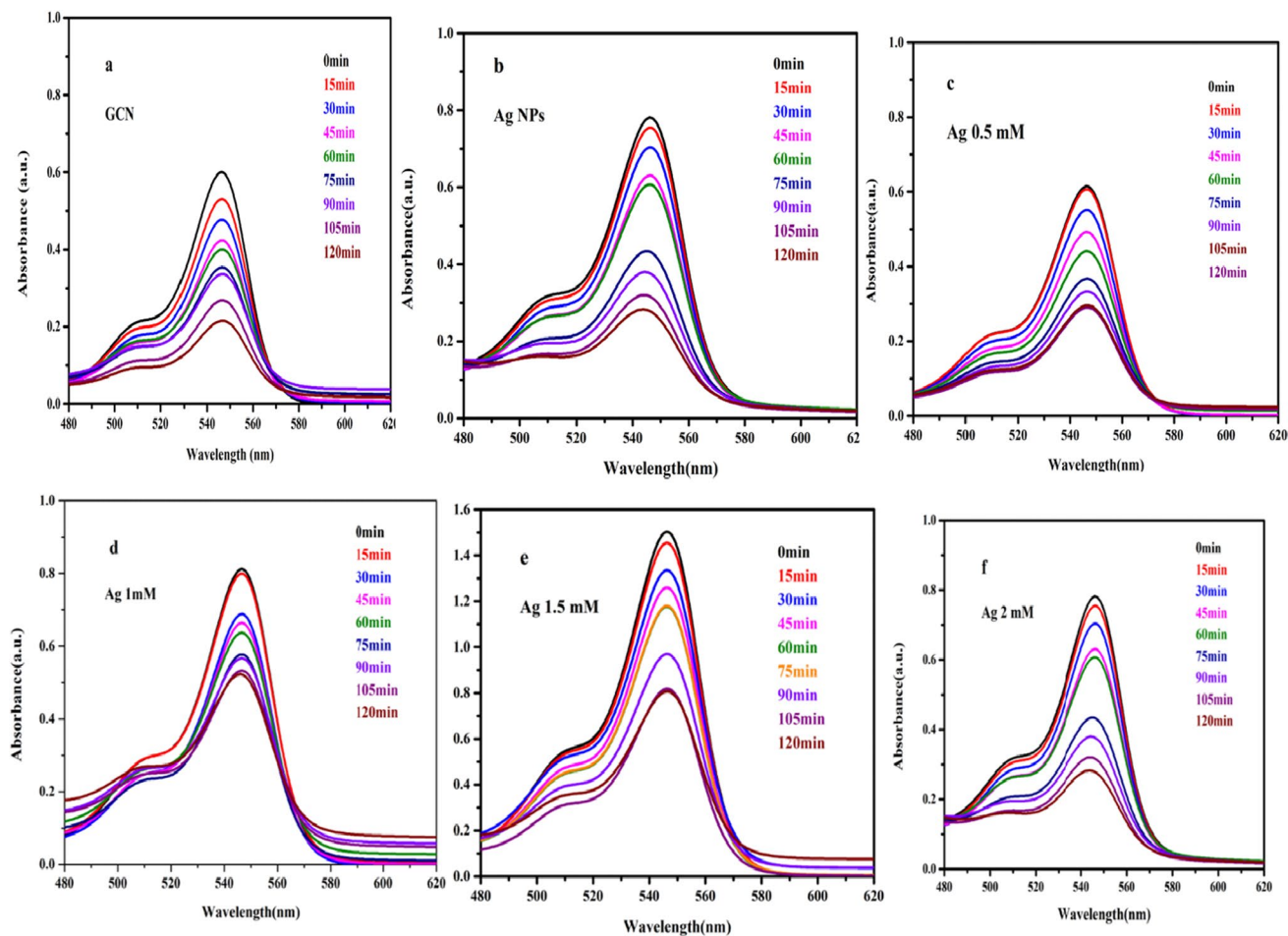


Fig. 9 UV degradation spectra of RB dye of **a** GCN, **b** Ag-NPs, and **c–f** Ag-doped GCN NCs at varied conc

with variable time intervals. The absorption peaks of RB and XO dyes reduced with an increase in time when Ag-NPs were used as the catalyst (Figs. 9 and 10).

The XO dye shows a broad peak and flattened absorbance spectra as compared to RB dye. The degradation efficiency of XO is less than RB dye at diff. conc. of nanocomposites as shown in Fig. 12. The RB dye being cationic in nature and its degradation capability get enhanced due to the positive charge of Ag-NPs, as they provide more surface to cationic RB dyes (Ghazali et al. 2022). This may also be due to the Cl⁻ and ONa⁺ group in the dye structure, which imparts a positive charge during its breakdown in the water.

Conclusion

This research work prepared a novel series of Ag-doped GCN photocatalysts using *Ocimum tenuiflorum* (Tulsi) leaf extract as a one-step green synthesis process. The

dye degradation efficiency of pure GCN for RB and XO was found to be 54% and 15%, respectively. When the Ag-NPs were doped into GCN (Ag-doped GCN nanocomposites) in varied conc. 0.5 mM, 1.0 mM, 1.5 mM, and 2.0 mM, respectively, it accelerated the photocatalytic efficiency of GCN from 54 to 76% for RB and 15 to 36% in the case of XO dyes. The maximum photocatalytic degradation efficiency was obtained when conc. of Ag-NPs in the GCN was 1.5 mM. It was 1.40 times higher than pure GCN for RB dye degradation and 2.4 times for XO dye degradation. The apparent rate constant of Ag 1.5 mM also increased from 0.007856 to 0.009211, which may be due to interfacial electron transmission, in Ag-doped GCN nanocomposites as it leads to greater separation of photogenerated charge carriers by enhancing charge carrier separation, and delaying photoinduced e⁻ h⁺. Thus, we can conclude that Ag-doped GCN nanocomposite has the potential to facilitate the development of a new-generation photocatalytic material with promising applications in wastewater treatment. The green route

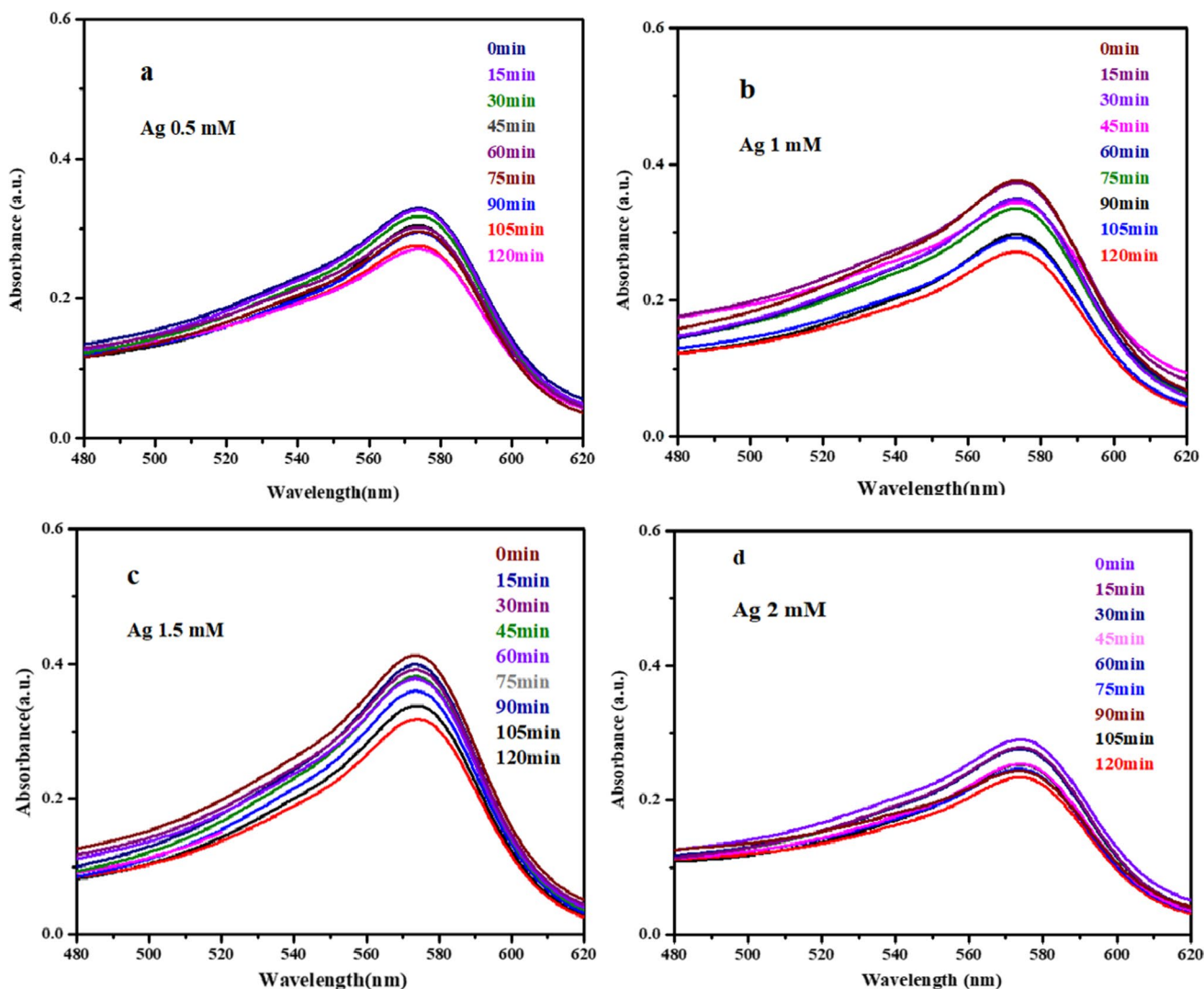


Fig. 10 UV degradation spectra of XO dye of Ag-doped GCN NCs at different concentrations

Table 2 Apparent rate constant and degradation efficiency of dyes

S.No.	Samples	Degradation efficiency of rose bengal dye (%)	Degradation efficiency of xylenol orange (%)	Apparent rate constant (<i>k</i>) min ⁻¹
1.	Ag-NPs	62	19	0.007211
2.	GCN	54	15	0.007856
3.	Ag 0.5 mM	45	15	0.001166
4.	Ag 1.0 mM	58	23	0.003921
5.	Ag 1.5 mM	76	36	0.009211
6.	Ag 2.0 mM	60	20	0.005304

synthesized nanocomposites are expected to minimize things that contribute to environmental problems and

offer a cost-effective, eco-benign, and energy-efficient green alternative.

Fig. 11 Photocatalytic mechanism of Ag-doped GCN photocatalyst

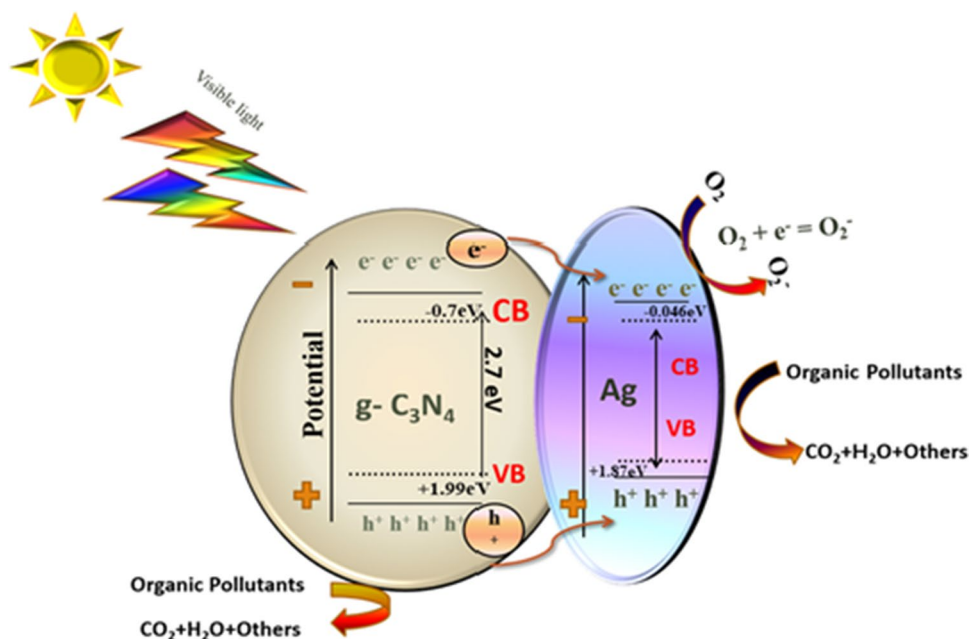
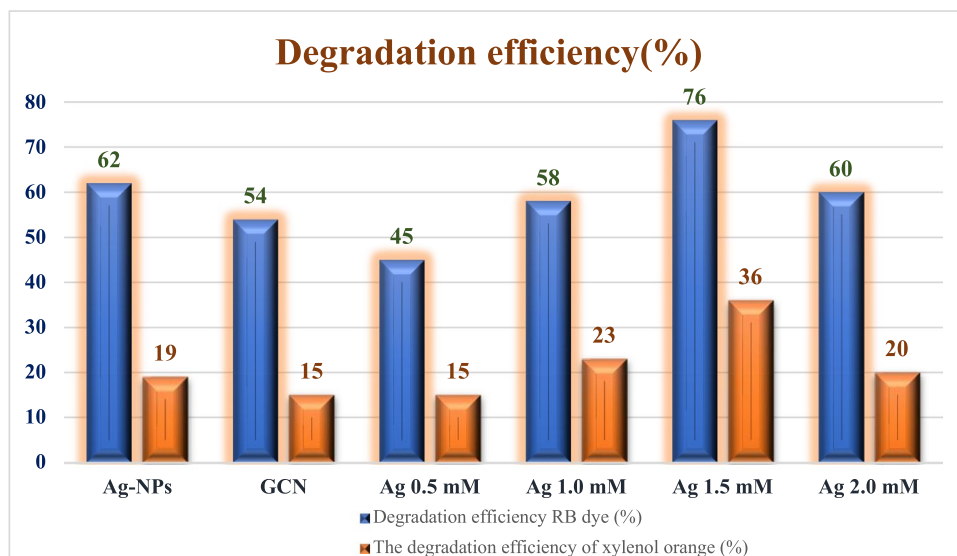


Fig. 12 Degradation efficiency of RB and XO dyes



Acknowledgements The authors are thankful to the Central Instrumentation Facility—Lovely Professional University (LPU), for providing characterization facilities.

Author contribution All authors contributed to the study conception and design.

Sweety: conceptualization, methodology, validation, roles/writing—original draft.

Anshu Sharma: supervision, conceptualization, methodology, roles/writing—original draft, writing—review and editing.

Sudesh Chaudhary: supervision, conceptualization, methodology, roles/writing—original draft; writing—review and editing.

Funding The author Sweety Dahiya (Endst. No. DCRUST/Sch./2021/612–617) is grateful to Deenbandhu Chhotu Ram University of Science and Technology, Murthal, for providing University Research Fellowship. Anshu Sharma acknowledges the University Grants Commission, Ministry of Education, Govt. of India, for providing Start-Up-Grant, reference no. 30–545/2021 (BSR).

Data availability Supplementary data and material will be published as received from the author.

Declarations

Ethical approval The research submitted is carried out in compliance with relevant institutional biosafety and biosecurity protocols.

Consent to participate Informed consent was obtained from all individual participants included in the study.

Consent for publication The authors affirm that participants provided informed consent for the publication of all images in Figures.

Competing interests The authors declare no competing interests.

References

- Ahmed S, Ahmad M, Swami BL, Ikram S (2016) A review on plants extract mediated synthesis of silver nanoparticles for antimicrobial applications: a green expertise. *J Adv Res* 7:17–28. <https://doi.org/10.1016/j.jare.2015.02.007>
- Bhakya S, Muthukrishnan S, Sukumaran M, Muthukumar M (2016) Biogenic synthesis of silver nanoparticles and their antioxidant and antibacterial activity. *Appl Nanosci* 6:755–766. <https://doi.org/10.1007/s13204-015-0473-z>
- Bhatia D, Sharma NR, Singh J, Kanwar RS (2017) Biological methods for textile dye removal from wastewater: a review. *Crit Rev Environ Sci Technol* 47:1836–1876. <https://doi.org/10.1080/10643389.2017.1393263>
- Buzea C, Pacheco I, Robbie K (2007) Nanomaterials and nanoparticles: sources and toxicity. *Biointerphases* 2(4):MR17–MR71. <https://doi.org/10.1116/1.2815690>
- Cao J, Zhao Y, Lin H, Xu B, Chen S (2013) Ag/AgBr/g-C₃N₄: A highly efficient and stable composite photocatalyst for degradation of organic contaminants under visible light. *Mater Res Bull* 48:3873–3880. <https://doi.org/10.1016/j.materresbull.2013.05.120>
- Cuerda-correa EM, Alexandre-franco MF, Fern C (2020) Antibiotics from water. An overview. *Water* 12:102
- Dai L, Liu R, Hu LQ, Si CL (2017) Simple and green fabrication of AgCl/Ag-cellulose paper with antibacterial and photocatalytic activity. *Carbohydr Polym* 174:450–455. <https://doi.org/10.1016/j.carbpol.2017.06.107>
- Daupor H, Chenea A (2017) Degradation of blue and red inks by Ag/AgCl photocatalyst under UV light irradiation. *AIP Conference Proceeding* 1868(020009):1–8. <https://doi.org/10.1063/1.4995095>
- Fan Y, Bao Y et al (2018) Controllable synthesis of coloured AgO/AgCl with spectral analysis for photocatalysis. *RSC Advances* 8(44):24812–24818. <https://doi.org/10.1039/c8ra04180f>
- Gaballah MS, Abdelwahab O, Barakat KM, Aboagye D (2020) A novel horizontal subsurface flow constructed wetland planted with *Typha angustifolia* for treatment of polluted water. *Environ Sci Pollut Res* 27:28449–28462. <https://doi.org/10.1007/s11356-020-08669-5>
- Ge L, Han C, Liu J, Li Y (2011) Enhanced visible light photocatalytic activity of novel polymeric g-C₃N₄ loaded with Ag nanoparticles. *Appl Catal A Gen* 409–410:215–222. <https://doi.org/10.1016/j.apcata.2011.10.006>
- Ge J, Chen Y, Xu J, Liu Y, Zhang L, Zha F (2019) Fabrication of Ag@AgCl with enhanced plasmonic photocatalysis performance via a deep eutectic solvent. *Aust J Chem* 72:200–205. <https://doi.org/10.1071/CH18386>
- Ghazali SZ, Mohamed Noor NR, Mustaffa KMF (2022) Anti-plasmodial activity of aqueous neem leaf extract mediated green synthesis-based silver nitrate nanoparticles. *Prep Biochem Biotechnol* 52:99–107. <https://doi.org/10.1080/10826068.2021.1913602>
- Jadoun S, Arif R, Jangid NK, Meena RK (2021) Green synthesis of nanoparticles using plant extracts: a review. *Environ Chem Lett* 19:355–374. <https://doi.org/10.1007/s10311-020-01074-x>
- Karagolge Z, Gur B (2016) Sustainable chemistry: green chemistry. *Iğdır University J Instr Sci Technol* 6(2):89–96. <https://doi.org/10.21597/jist.2016218851>
- Katas H, Moden NZ et al (2018) Biosynthesis and potential applications of silver and gold nanoparticles and their chitosan-based nanocomposites in nanomedicine. *J Nanotechnol* 2018:1–13. <https://doi.org/10.1155/2018/4290705>
- Liu C, Wang L, Xu H, Wang S, Gao S, Ji X, Xu Q et al (2016) “one pot” green synthesis and the antibacterial activity of g-C₃N₄/Ag nanocomposites. *Mater Lett* 164:567–570. <https://doi.org/10.1016/j.matlet.2015.11.072>
- Liu R, Yang W, He G, Zheng W, Li M, Tao W, Tian M (2020) Ag-modified g-C₃N₄ prepared by a one-step calcination method for enhanced catalytic efficiency and stability. *ACS Omega* 5:19615–19624. <https://doi.org/10.1021/acsomega.0c02161>
- Martín-Ramos P, Martín-Gil J, Dante RC, Vaquero F, Navarro RM, Fierro JLG (2015) A simple approach to synthesize g-C₃N₄ with high visible light photoactivity for hydrogen production. *Int J Hydrogen Energy* 40:7273–7281. <https://doi.org/10.1016/j.ijhydene.2015.04.063>
- Meng Y, Shen J, Chen D, Xin G (2011) Photodegradation performance of methylene blue aqueous solution on Ag/g-C₃N₄ catalyst. *Rare Met* 30:276–279. <https://doi.org/10.1007/s12598-011-0284-7>
- Panchal P, Paul DR, Sharma A, Hooda D, Yadav R, Meena P, Nehra SP (2019) Phytoextract mediated ZnO/MgO nanocomposites for photocatalytic and antibacterial activities. *J Photochem Photobiol A Chem* 385:112049. <https://doi.org/10.1016/j.jphotochem.2019.112049>
- Paul DR, Sharma R, Panchal P, Malik R, Sharma A, Tomer VK, Nehra SP (2019) Silver doped graphitic carbon nitride for the enhanced photocatalytic activity towards organic dyes. *J Nanosci Nanotechnol* 19:5241–5248. <https://doi.org/10.1166/jnn.2019.16838>
- Paul DR, Sharma R, Panchal P, Nehra SP, Gupta AP, Sharma A (2020) Synthesis, characterization and application of silver doped graphitic carbon nitride as photocatalyst towards visible light photocatalytic hydrogen evolution. *Int J Hydrogen Energy* 45:23937–23946. <https://doi.org/10.1016/j.ijhydene.2019.06.061>
- Qu X, Alvarez PJJ, Li Q (2013) Applications of nanotechnology in water and wastewater treatment. *Water Res* 47:3931–3946. <https://doi.org/10.1016/j.watres.2012.09.058>
- Rattan Paul D, Nehra SP (2021) Graphitic carbon nitride: a sustainable photocatalyst for organic pollutant degradation and antibacterial applications. *Environ Sci Pollut Res* 28:3888–3896. <https://doi.org/10.1007/s11356-020-09432-6>
- Sengupta A, Sarkar A (2022) Synthesis and characterization of nanoparticles from neem leaves and banana peels: a green prospect for dye degradation in wastewater. *Ecotoxicology* 31:537–548. <https://doi.org/10.1007/s10646-021-02414-5>
- Sharma R, Saini H, Paul DR, Chaudhary S, Nehra SP (2021) Removal of organic dyes from wastewater using *Eichhornia crassipes*: a potential phytoremediation option. *Environ Sci Pollut Res* 28:7116–7122. <https://doi.org/10.1007/s11356-020-10940-8>
- Shoran S, Chaudhary S, Sharma A (2022) Photocatalytic dye degradation and antibacterial activities of CeO₂/g-C₃N₄ nanomaterials for environmental applications. *Environ Sci Pollut Res*. <https://doi.org/10.1007/S11356-022-23815-X>

- Singh J, Dutta T, Kim KH, Rawat M, Samddar P, Kumar P (2018) “Green” synthesis of metals and their oxide nanoparticles: applications for environmental remediation. *J Nanobiotechnology* 16:1–24. <https://doi.org/10.1186/s12951-018-0408-4>
- Soltani N, Saion E, Hussein MZ, Erfani M, Abedini A, Bahmanrokh G, Navasery M et al (2012) Visible light-induced degradation of methylene blue in the presence of photocatalytic ZnS and CdS nanoparticles. *Int J Mol Sci* 13:12242–12258. <https://doi.org/10.3390/ijms131012242>
- Vinodkumar T, Subramanyam P, Kumar KVA, Reddy BM, Subrahmanyam C (2019) Construction of metal oxide decorated g-C₃N₄ materials with enhanced photocatalytic performance under visible light irradiation. *J Chem Sci* 131:1–11. <https://doi.org/10.1007/s12039-018-1588-z>
- Wang J, Da L, Song K, Li BL (2008) Temporal variations of surface water quality in urban, suburban and rural areas during rapid urbanization in Shanghai, China. *Environ Pollut* 152:387–393. <https://doi.org/10.1016/j.envpol.2007.06.050>
- Wang T, Jin X, Chen Z, Megharaj M, Naidu R (2014) Green synthesis of Fe nanoparticles using eucalyptus leaf extracts for treatment of eutrophic wastewater. *Sci Total Environ* 466–467:210–213. <https://doi.org/10.1016/j.scitotenv.2013.07.022>
- Zada A, Muhammad P et al (2019) Surface plasmonic-assisted photocatalysis and optoelectronic devices with noble metal nanocrystals: design, synthesis, and applications. *Adv Funct Mater* 30(7),1906744:1–29 <https://doi.org/10.1002/adfm.201906744>

Publisher's note Springer Nature remains neutral with regard to jurisdictional claims in published maps and institutional affiliations.

Springer Nature or its licensor (e.g. a society or other partner) holds exclusive rights to this article under a publishing agreement with the author(s) or other rightsholder(s); author self-archiving of the accepted manuscript version of this article is solely governed by the terms of such publishing agreement and applicable law.